The energetics of the acetylation switch in p53-mediated transcriptional activation

Kenneth D. Eichenbaum,[1] Yoel Rodríguez,[1,2] Mihaly Mezei,[1] and Roman Osman[1]*

[1] Department of Structural and Chemical Biology, Mount Sinai School of Medicine, New York University, One Gustave L. Levy Place, New York, New York 10029

[2] Department of Natural Sciences, Hostos Community College of CUNY, Bronx, New York 10451

ABSTRACT

Targeted therapeutic intervention in receptor-ligand interactions of p53-mediated tumor suppression can impact progression of disease, aging, and variation in genetic expression. Here, we conducted a number of molecular simulations, based on structures of p53 in complex with its transcriptional coactivating CBP bromodomain, determined by NMR spectroscopy, to investigate the energetics of the binding complex. Building on the observation that acetylation of K382 in p53 serves as the essential triggering switch for a specific interaction with CBP, we assessed the differential effect of acetylation on binding from simulations of an octapeptide derived from p53 with acetylated and nonacetylated K382 (residues 379–386). Cluster analysis of the simulations shows that acetylation of the free peptide does not significantly change the population of the preferred conformation of the peptide in solution for binding to CBP. Conversion of the acetylated K382 to nonacetylated form with free energy perturbation (FEP) simulations of the p53 CBP complex and the free peptide showed that the relative contribution of the acetyl group to binding is 4.8 kcal/mol. An analysis of residue contributions to the binding energy using an MM-GBSA approach agrees with the FEP results and sheds additional light on the origin of selectivity in p53 binding to the CBP bromodomain.

INTRODUCTION

Characterizing the activation mechanisms of p53 tumor suppressor activity can provide insight into developing targeted intervention strategies against cancer progression. p53, often referred to as "the guardian of the genome,"[1] is a protein containing 393 amino acids, with functional domains responsible for cellular activities that include transcriptional activation, DNA repair, G_1/S checkpoint growth regulation, initiation of apoptosis, and senescence. The importance of p53 in cancer is highlighted by the fact that its altered expression is observed in over 50% of human tumors.[2,3] p53 is believed to exert its influence over gene activation and silencing at the chromatin level in an epigenetic modality, using histone-directed lysine acetylation signaling pathways.[4] Because p53 is active in both cell cycle regulation and tumor suppressor activity, a molecular understanding of its binding selectivity can facilitate the design of specific small molecule ligands that can bind and regulate its epigenetic activity.[5]

A primary regulator of p53 stability is the p53-interacting protein MDM2.[6] MDM2, whose expression is controlled through negative feedback by p53 itself, forms a complex with p53, thereby reducing tumor suppression activity in unstressed cells. For example, in murine studies, MDM2 homozygous deletion resulted in apoptosis and embryonic death; simultaneous deletion of MDM2 and p53 yielded apparently normal growth and development, but increasingly prone to tumors from lack of p53 tumor suppression.[7–9] MDM2-bound p53 inhibits p53-mediated transcription by preventing p53 from contacting transcriptional coactivators such as p300 and CBP and subsequently allows for p53 export from the nucleus to the cytoplasm via the ubiquitination proteasome system.[9]

Upon MDM2 dissociation from p53, the evolutionarily conserved bromodomain, an atypical left-handed four-helix bundle found in transcriptional coactivating proteins such as CBP, p300, and histone acetyltransferases, plays a unique role in its ability to bind to acetyl-lysine motifs in histones and proteins.[10] By binding to acetyl-lysines and histones, bromodomains can govern the molecular interactions between proteins in histone-regulated chromatin modeling and gene transcription. Bromodomains

may act by tethering nuclear histone acetyltransferases (HATs) to distinct chromosomal sites.[11–13] In particular, CBP bromodomain recognition of p53•K382ac, as opposed to other lysine acetylation sites, may function as a chemical switch, which controls target transcriptional activation of cyclin-dependendent kinase inhibitor p21 in cell cycle arrest.[10,14,15] The ability to decrease p53-mediated p21 activation has been demonstrated experimentally.[16] In this way, post-translational modifications of p53 can mediate its signaling pathways.[14]

Woods and Vousden suggested that the conformation of p53 C-terminus is potentially a critical regulator of p53 binding selectivity.[9] The implication is that binding selectivity could be in part determined by the conformational properties of the p53 C-terminal peptide, that is, the acetylated form is more likely to bind bromodomain proteins because it has the correct conformation, whereas the nonacetylated lysine does not achieve favorable binding conformation. A *priori*, we can argue that the binding energy is the result of two effects: (1) the energy required to adapt the peptide from its conformation(s) in solution to that in the form bound to CBP; (2) the free energy of interaction of the peptide with CBP. So far as we know, there are no experimental data about the conformational states of native and acetylated p53 or peptides derived from it. Recent molecular dynamics (MD) simulations on histone peptides lead to a conclusion that post-translational changes do not affect the conformation of the peptides in a significant manner.[17] To evaluate the contribution of the putative conformational rearrangement of the peptide, we describe our investigation of the difference in conformational properties of the acetylated and nonacetylated peptides. To assess the contribution of the acetylated form of K382, we evaluate the relative energy by a free energy perturbation method in which the acetylated K382 was mutated to the nonacetylated form in solution and in complex with the CBP bromodomain. Based on similar results from Molecular Mechanics-Poisson Boltzman (Generalized Born) Surface Area (MM-PB(GB)SA),[18,19] we analyze the contributions of other residues of the p53 peptide to binding.

METHODS

Molecular systems

To study the conformational properties of the peptide proximal to the acetylated ligand site, we isolated a p53 octapeptide residue sequence (residues 379–386; Arg-His-Lys-AcLys-Leu-Met-Phe-Lys) surrounding K382 from the NMR structure (PDB id 1JSP). The terminal residues were blocked by an acetyl group on the amino terminus and by NHCH₃ on the carboxy terminus. The simulations of the complex p53 with CBP bromodomain were conducted on native structure obtained from NMR in which the peptide was also truncated to the same eight residues.

Molecular dynamics simulations

All simulations were performed with NAMD v2.6[20] using the CHARMM22 force field.[21] The force field for the acetyl lysine residue (Kac) was made using the CHARMM22 force field. The ACE patch was used for the acetyl group in the Kac residue. The amide linkage between NZ of lysine and carbonyl carbon CY of ACE was created in the same way as acetylation at the N-terminus of amino acids. The NZ and HNZ charges used were $-0.47e$ and $0.31e$, respectively. The charge on CE was assigned to $0.06e$ (similar to that of CA bound to an acetyl group at the N-terminus) and the charges of HE atoms were $0.05e$. The remaining charges were the same as for a standard lysine. No new bonding or van der Waals (vdW) parameters were needed.

The systems were set up at neutral pH and an ionic strength of $0.15M$ using Na^+ and Cl^- ions in the auto-ionize module of visual molecular dynamics (VMD) program.[22] The systems were solvated in a periodic box, energy minimized for 500 steps without restraints using a dielectric constant of 1.0, with a vdW cutoff of 12 Å, a switching distance of 10.0 Å and a pairlist distance cutoff of 14.0 Å. Electrostatic interactions were evaluated with the Particle Mesh Ewald method with a tolerance of 10^{-6}. The SHAKE algorithm[23] was utilized for all bonds to hydrogens with a tolerance of 10^{-6}. Simulations were initiated at zero temperature and heated to 300 K in a single linear ramp at 10 K/ps. Molecular dynamics (MD) production runs were done at constant pressure and temperature (NPT ensemble) with Berendsen's coupling method. The p53 complex with the CBP bromodomain was set up with 10 Na^+ and 9 Cl^- ions and solvated in a periodic box 80 Å × 54 Å × 54 Å containing 6440 water molecules. The octapeptide simulation included about 1800 water molecules in a rectangular simulation cell approximately 37 Å × 40 Å × 43 Å. During NPT simulations, the average density was 1.0117 g/cm³.

MD simulations of the octapeptide were run for 40 ns on an AppleG5 cluster at Mount Sinai School of Medicine. The simulation of the complex was run at the Texas Advanced Computing Center (TACC) for a duration of 20 ns.

Conformational analysis

The conformational analysis of the peptide trajectories was conducted with the program Simulaid.[24] The evolution of the backbone torsion angles φ and ψ were displayed in dial plots[24,25] that are well suited for the characterization of the extent of sampling of these angles, as well as for the propensity of each residue toward specific conformation(s), if any (see Fig. 2). However, torsional

space is ill suited for clustering of populations in linear peptides. Thus, a different approach for the characterization of the conformational ensembles was based on the two dimensional root-mean-square deviation (2D RMSD) plot, the matrix of the RMSD values calculated between each pair of conformations extracted from the trajectory after minimizing the difference by overlaying the pair of structures.[26] These 2D RMSD values were used to cluster the structures of each trajectory using a variant of the K-means clustering method. This method produces K clusters by iteratively optimizing the cluster centroids (one member of the cluster) starting from an initial set of K structures as centroids. Each structure is assigned to the cluster whose putative centroid is the nearest to it. In subsequent iterations, new centroids are calculated until convergence. Because our distance measure is the RMSD obtained after optimal overlay of structure pairs, it is not amenable to deriving a meaningful average to be used as the putative centroid in the next iteration. Instead, we chose the structure, whose largest RMSD with the rest of the cluster member is the smallest, as the new centroid.

The clusters obtained from the two octapeptide simulations were compared by mapping each cluster obtained from one simulation onto the clusters of the second simulation. For example, mapping cluster i_2 of simulation 1 to cluster j_3 of simulation 2 is equivalent to counting the number of configurations in cluster i_2 whose RMSD from the center of cluster j_3 is within a specified threshold value.

Free energy perturbation

The FEP simulations were conducted using the alchemical Free Energy Perturbation implemented in NAMD v 2.6.[27] A hybrid residue A2K was constructed in a dual topology such that the acetylated nitrogen NZ of K382 (K382ac residue) was converted to a native lysine. It is noteworthy that such an alchemical change, in addition to eliminating the entire acetyl group, also creates a positive charge on the terminal NZ. Because NAMD does not allow to conduct PME simulations with a change in the total charge of the system, the simulations were conducted with a cutoff on electrostatic interactions of 12 Å. We have shown previously that the potential contributions from the unbalanced electrostatics are negligible.[28] We used the recommended FEP protocol described by Henin and Chipot[27] with the following parameters. All simulations were conducted with a time step of 1 fs. The initial segments where appearance/disappearance of new atoms was taking place were run with the following λ values: {0.0000001, 0.000001, 0.00001, 0.0001, 0.001, 0.01, 0.05, 0.1}. Between 0.1 and 0.9, the change in λ was linear with dλ of 0.1. At the final segments, the progression of λ was {0.9, 0.95, 0.99, 0.999, 0.9999, 0.99999, 0.999999, 0.9999999}. Each segment was equilibrated for

40 ps and MD data were accumulated for 200 ps. The total time for each FEP was 5.28 ns. The simulations were run forward, that is, mutating Kac→K, as well as backward to estimate the error in the procedure.

Interaction energy decomposition

We used the method of Gohlke *et al.*[29,30] to decompose the interaction energy into residue-based components. In this approach, the interaction energy between the p53-peptide and the CBP bromodomain was decomposed in an additive fashion according to the MM-PB(GB)SA scheme. The MM term is composed of the vdW and electrostatic interactions between each residue in the peptide and all the residues in the CBP bromodomain. Similarly, the change in solvation energy was estimated as a sum of the GB and the surface area components associated with each residue. The total MM-GBSA energy is the sum of the MM and the GBSA components. Furthermore, the residue-associated energies were decomposed into contributions from the side chain and the backbone. The entropic contributions from changes in vibrational, translational, and rotational entropies cannot be decomposed into residue-based components and thus were not included in the analysis. All constituent contributions represent averages from evenly spaced 100 configurations extracted from the MD trajectories.

Inter-residue contact analysis

The time course of three different types of contacts were extracted from the simulation trajectories: (a) salt bridges, defined as oppositely charged heavy atoms within 5.0 Å, (b) hydrophobic interactions, defined as two aliphatic carbons within 4.0 Å, and (c) hydrogen bonds, defined as a donor with a nonaliphatic hydrogen and acceptor pair satisfying the following conditions: (1) the donor–acceptor distance square is less than $1.4 \times R_{vdW}^2$ where R_{vdW} is 1.68 for nitrogen and oxygen and 1.8 for sulphur; (2) the Acceptor…H-Donor angle is greater than 90°. The time course of each type of contact was condensed into residue:residue interaction map where for each residue pair the fraction of time they were in contact was determined. The analysis was performed with the program Simulaid.[24]

RESULTS AND DISCUSSION

Conformational properties of acetylated and nonacetylated p53 octapeptide

To determine whether differences in conformational propensity of the unbound peptide contribute to the preferential binding of the acetylated peptide, the conformations sampled during the simulations of the two peptides were compared at two levels. At the level of the backbone conformations, we computed dial plots[31] for
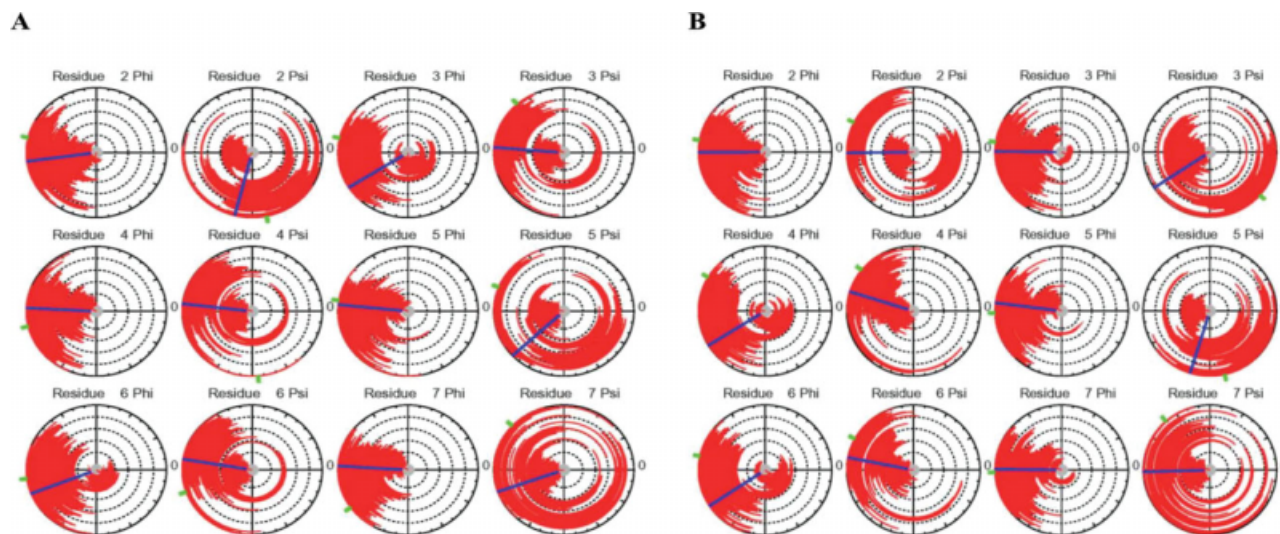
Figure 1

Radial dial plots for each {φ, ψ} angle spanning the p53 octapeptide. Each concentric circle extending outward from the center represents 4.0 ns and the angle is tracked by the red line extending outward from the center. The line in the small central gray disc shows the initial value of the angle, the blue line indicates the average angle calculated over the course of the trajectory, and the green tick mark outside the dial shows the final value of the angle. (**A**) Acetylated lysine; (**B**) Nonacetylated lysine. [Color figure can be viewed in the online issue, which is available at www.interscience.wiley.com.]

each φ and ψ angle spanning the octapeptide, using simulaid. These radial plots depict the values of the φ or ψ angle as a function of time in the simulation along the radial direction outward from the center and each concentric circle of increasing radius represents 4 ns of simulation time. The azimuthal coordinate represents the value of the angle. Figure 1(a,b) show the dial plots for the acetylated and nonacetylated octapeptide simulations (**S1** and **S2**), respectively. The radial plots show that the distributions of the φ angles were mostly unimodal with the averages positioned around −90°. The ψ angles show usually two populations near 60° and 150° with varying occupancies. The fluctuations in the angles suggest that sampling was extensive. A closer examination of the distributions shows that upon removing the acetyl group on K382, the main changes in populations occur at ψ_2, ψ_4, and ψ_5. However, because changes in some of the angles appear to be correlated with others, we decided to characterize the ensembles by clustering the populations according to the RMSD between the structures in the simulation.

Examination of the 2D-RMSD plots for simulations **S1** and **S2** suggested that both simulations sampled three clusters at RMSD threshold of 2.5 Å. The 2D-RMSD plot for simulation **S1** is shown in Figure 2, in which the structures are sorted by cluster membership, and the different clusters are delineated by a black line. The cluster membership as a function of simulation time is shown in Figure 3(a,b) for simulations **S1** and **S2**, respectively. Both simulations show extensive crossings among the clusters, suggesting reasonably adequate sampling. To corroborate this conclusion, we divided the trajectory of the acetylated p53 into two segments of 20 ns each and compared their cluster membership using a cross-RMSD analysis. Each trajectory was clustered into three clusters, which contained 96, 177, and 227 members from the first half of the trajectory and 183, 200, and 117 in the second half. A comparison of cross membership shows that all the members of cluster 2 from the second half belong to cluster two of the first half. Thus, the change in population is from 177 in the first segment to 200 in the second. Similar results apply to the nonacetylated peptide (207 members out of 214 of the second half coincide with a cluster counting 144 members in the first half). These data indicate that sampling is reasonable and relatively stable during the simulations, although demonstrating convergence would require a much more extensive analysis.

To relate the conformations of the K382ac-octapeptide sampled during the simulation to the structures predicted by NMR, the 20 structures NMR of the NMR ensemble were combined into a pseudo trajectory, and the cross-RMSD's were calculated between simulation **S1** and the NMR ensemble. The three clusters of simulation **S1** were mapped (using a 3 Å RMSD threshold) on the NMR ensemble that was considered to form a single cluster. Although 76% of cluster 1 mapped on the NMR ensemble, only 33 and 37% of clusters 2 and 3, respectively, mapped on the NMR ensemble, suggesting that cluster 1 is the most NMR-like. Overall, using the 3 Å RMSD threshold, 52% of the structures in simulation **S1** were mapped on the NMR ensemble.
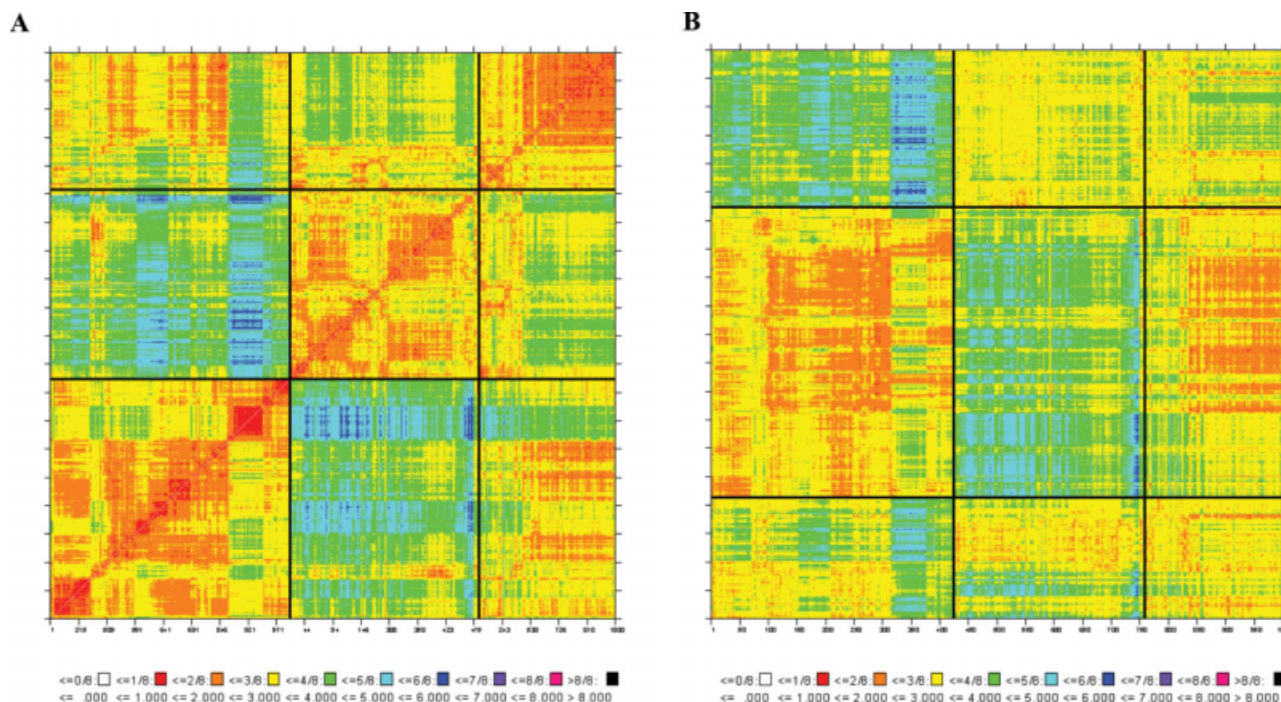
Figure 2

A: 2D-RMSD map of the aceytlated p53 octapeptide simulation sorted by clusters demarcated by black lines (see text for clustering methodology and populations). **B:** Cross-RMSD map between the simulations of octapeptides with acetylated (vertical axis) and nonacetylated lysine (horizontal axis) sorted by clusters demarcated by black lines.

The calculated cross-RMSD map, using the cluster-sorted order of snapshots, is depicted in Figure 2, which shows that the two largest clusters (cluster 1 of **S1** and cluster 2 of **S2**) have the largest overlap. The centroid structures of the three ensembles, that is, structure 728 from **S1**, structure 606 from **S2**, and structure 10 from the NMR ensemble were superimposed and are shown in Figure 4. The similarity among the clusters of the two simulations is shown in Table I, confirming the close correspondence between cluster 2 of **S1** and cluster 1 of **S2**.
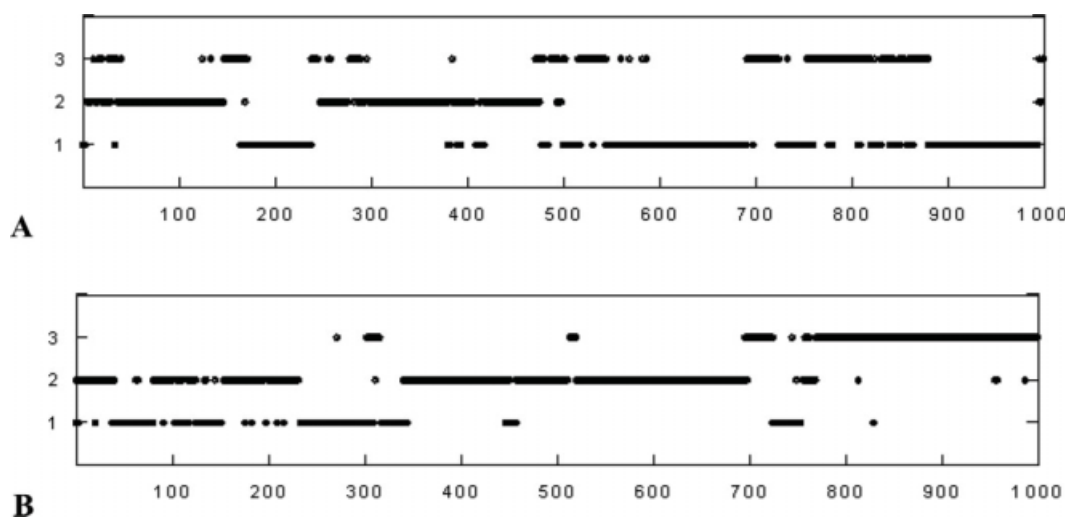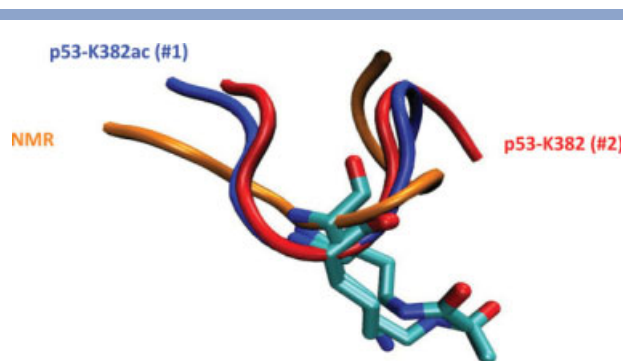

Figure 3

Cluster memberships and transitions as a function of time during the 40 ns peptide simulation. (**A**) Acetyleted lysine; (**B**) Nonacetylated lysine.

Figure 4
Superposition of structures from the centroids of the clusters on the NMR structures (orange backbone), K382ac-octapeptide (blue backbone), and the K382-octapeptide (red backbone).

For example, 438 structures of the 509 members of cluster 3 of simulation **S2** are classified as belonging to cluster 1 of simulation **S1**, which contains 424 structures. These numbers can be related to the free-energy difference between the ensembles represented by the clusters via the equation $\Delta G = -RT \ln(P_i/P_j)$ where the ratio P_i/P_j represents the relative probability of finding the peptide in conformations corresponding to cluster i and j. Because both trajectories consisted of the same number of structures, P_i/P_j can be approximated by N_i/N_j, where N_i and N_j are the number of structures in clusters i and j, respectively, leading to the approximation $\Delta G = -RT \ln(N_i/N_j) = -0.02$ kcal/mol. Even if all the members of simulation **S2** that can be classified to cluster 1 of **S1** are counted (i.e., 516), the free energy difference remains only -0.1 kcal/mol in favor of the K382-p53 structure. It is of interest to note that the largest cluster in each simulation is the one most similar both to each other and to the NMR ensemble. This result clearly indicates that the conformational differences between the acetylated and nonacetylated p53 do not contribute to the binding to CBP bromodomain. We conclude that the preferential binding depends on the interaction of the K382ac with its binding site.

Contribution of the acetyl group to p53 binding from FEP simulations

To test the importance of the acetyl group on K382 for p53 binding to the CBP bromodomain, we conducted FEP simulations in which the acetyl-lysine was converted to lysine in two separate simulations. In one, the conversion took place in the p53 octapeptide in solution and in the other in a complex with the CBP bromodomain. The FEP simulations were conducted in both directions, that is, from K382ac to K382 (forward) and from K382 to K382ac (reverse). The results in Figure 5 show that the forward and reverse simulations produce consistent

results with relatively small hysteresis. Clearly, the conversion in the peptide is less costly than in the complex with CBP, indicating that the acetyl group makes a substantial contribution to binding. Binding of the acetylated p53 peptide is preferred by 4.8 ± 0.5 kcal/mol over the nonacetylated peptide. The electrostatic and van der Waals interaction make nearly equal contributions to the free energy difference. It is more costly to convert a neutral acetyl group to a charged lysine in the complex than in solution, which may originate from the largely hydrophobic nature of the binding pocket. In addition, the elimination of the acetyl group contributes to a loss of vdW interactions. Although the exact values of the relative contribution of these interactions may depend on the specific details of the perturbation path, their values clearly are consistent with the nature of the interactions between the acetyl group and its binding pocket.[10] To illustrate the nature of the interactions between the acetylated and nonacetylated lysine, snapshots from the simulations with λ near 1 and 0 are shown in Figure 6.

Experimental confirmation for the predicted change in affinity may be difficult to obtain from direct experiments. Estimated affinity of the K382ac p53 octapeptide is 187 ± 23 μM,[11] which would result with an affinity of the nonacetylated peptide around 600 mM. The polybromo-1-bromodomains bind acetylated histone H3 with considerably higher affinity.[32] For example, the dissociation constants of K4ac, K9ac, and K14ac of H3 from various bromodomains of the polybromo are 0.39, 0.36, and 0.79 μM.[32] The authors estimated that the nonacetylated peptides bind with a mM dissociation constant, which is difficult to measure. The difference in binding free energy between the acetylated and nonacetylated peptides translates into a range of 4.3–4.9 kcal/mol, which is in excellent agreement with our FEP results.

Interactions and H-bonding between K382ac p53 and CBP bromodomain

We have examined the behavior of the various interactions within and between the molecules of the complex
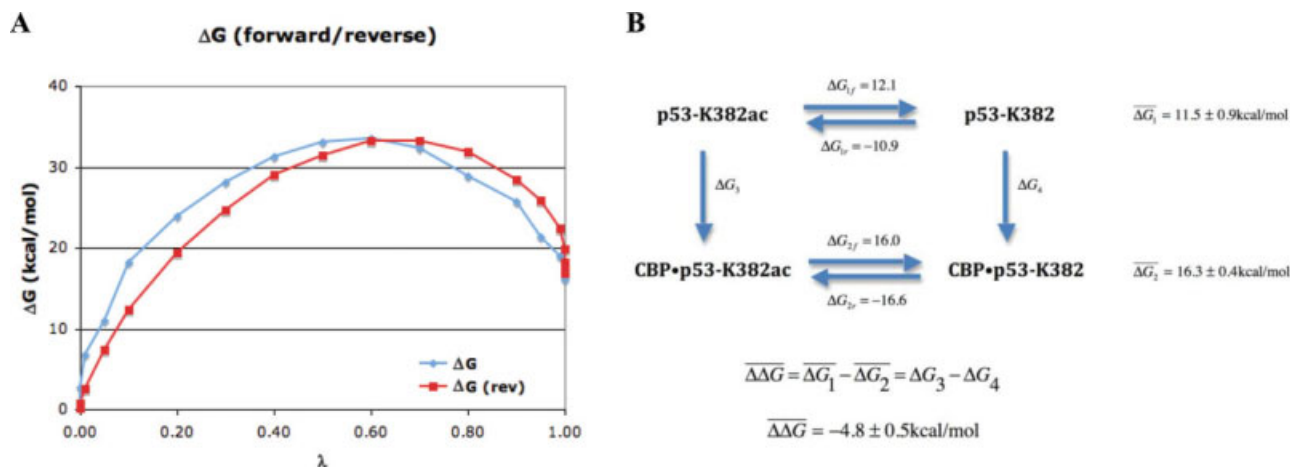
Table I
Characterization of Similarity Between Clusters of the Configurational Ensembles of Acetylated and Nonacetylated p53

	Cluster members in K382-p53[a]	Cluster 1	Cluster 2	Cluster 3
Cluster members in K382ac-p53[b]		424	334	242
Cluster 1	214	78[c]	47	89
Cluster 2	509	438	0	71
Cluster 3	277	0	155	122

[a]Number of members in the clusters of the p53●K382 in column.
[b]Number of members in the clusters of the p53●K382ac in row.
[c]Italicized numbers represent the number of members in clusters of p53●K382 that are classified to belong in clusters of p53●K382ac.
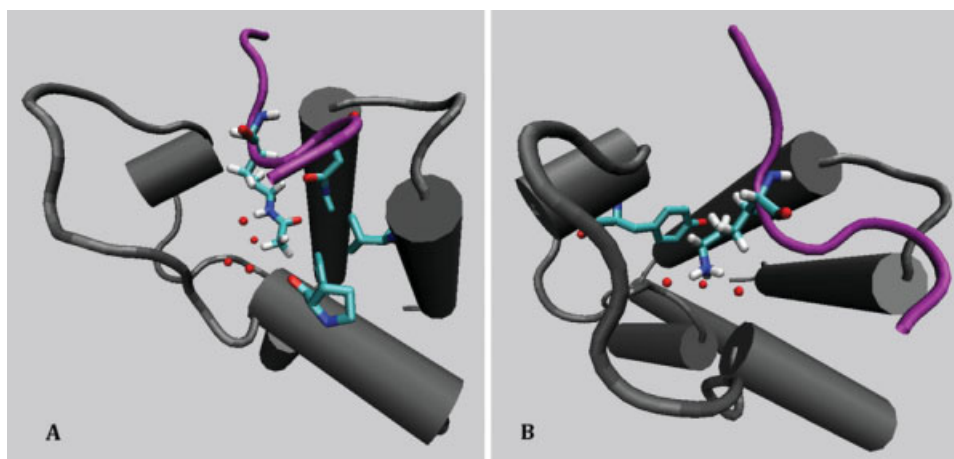
Figure 5

A: Free energy change as a function of λ in the forward and reverse directions. The curve in the reverse direction was shifted to align the values at λ = 0. **B**: Thermodynamic cycle representing the conversion of K382ac to K382 in the peptide and in complex with CBP. $\overline{\Delta\Delta G}$ and the errors are estimated from forward and reverse simulations. [Color figure can be viewed in the online issue, which is available at www.interscience.wiley.com.]
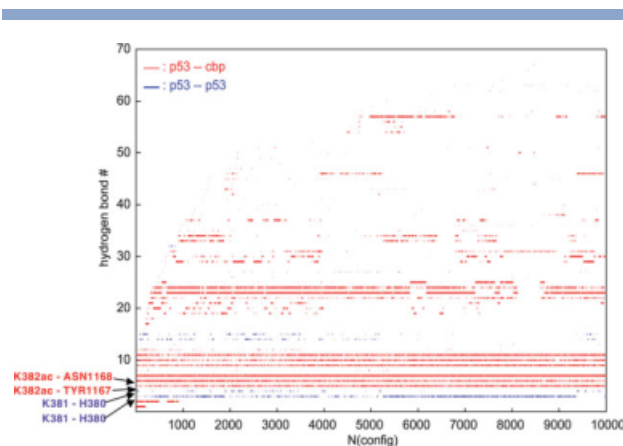
of p53 with CBP as a function of simulation time. The time course of the salt bridges between p53 and CBP shows a strong interaction between the first arginine residue in the peptide (R379) and D1124 in CBP, which persists for over 90% of the time. The C-terminal lysine in the octapeptide (K386) has a persistent interaction with E1105 in CBP (∼80%) and an intermittent interaction with D1107 (∼10%). No salt bridges were found between atoms from p53 and K381, the position directly preceding K382. No salt bridge is observed because there is a frequent hydrogen bonding interaction with H380. Additional hydrogen bonds between p53 and CBP are maintained throughout the simulations. Two are between K382ac in the peptide and key residues Y1167 and N1168 in the CBP bromodomain. An interesting hydrogen bond is formed for about 60% between the side chain OH of S1172 and the backbone carbonyl of L383 in the peptide.

Figure 7 shows the track of hydrogen bonds formed by p53 in the last 10 ns of the simulation of the complex as a function of time. The hydrogen bonds are numbered sequentially as they are formed in the course of the simulation. For example, Y1167 and N1168 in CBP form H-bonds with K382ac from the beginning and they persist

Figure 6

Snapshots from the FEP simulation showing the neighborhoods of K382ac and K382. **A**: Snapshot at λ near 1 showing the residues proximal to K382ac as well as the water molecules near the CH3 and N—H groups. **B**: Snapshot at λ near 0 showing the residues proximal to K382 as well as three water molecules H-bonded to the terminal ammonium group. [Color figure can be viewed in the online issue, which is available at www.interscience.wiley.com.]

Figure 7

Plot of the time evolution of hydrogen bonds in the p53•CBP complex. Each line represents a particular hydrogen bond, see Table I of the Supporting Information for the specification of each hydrogen bond. Breaks in a line represent a breakage of the hydrogen bond in that interval. Blue lines represent hydrogen bonds between atoms in p53 and red lines represent bonds between p53 and CBP.

throughout the simulation. On the other hand K381, which was not engaged in a salt bridge despite its charge, is shown to form two hydrogen bonds with the H380 of p53, which are intermittently broken and reformed. The hydrogen bonds corresponding to each track and their percent populations are described in Table I of the Supporting Information. As the order of hydrogen bonds in this plot (see Fig. 6) is the order they first formed during the simulation, the envelope of the marks for the hydrogen bond should level off for a well-converged simulation. This is indeed the case.

The extent of hydrophobic contacts between residues shows mainly two interactions of interest between the side chain of K382ac and Y1167 and V1174 in CBP. Their interactions persist for about 60–80%, while about half of the contacts appear less that 20% of the time, showing the extent of flexibility in the p53•CBP interaction.

Table II

Decomposition of Energetic Contributions (in kcal/mol) by Residues of the p53•K382ac Peptide

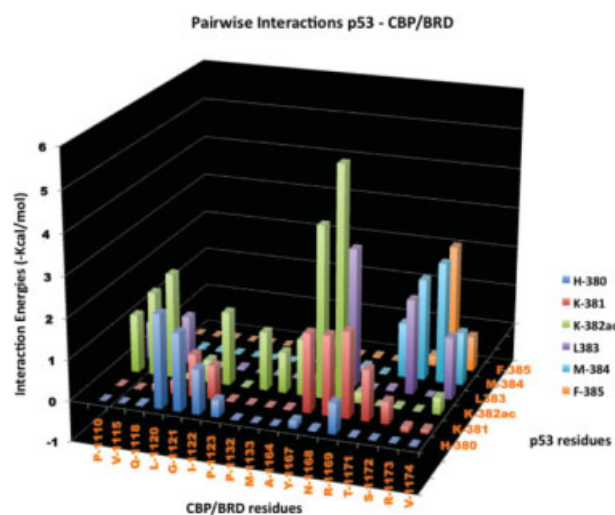|	Side chain	Backbone	Total	vdW	ELE	GB$_{SOL}$
R379	−5.7 ± 1.6	−0.5 ± 0.8	−5.2 ± 1.8	−0.2	−53.6	48.7
H380	−1.2 ± 0.8	0.2 ± 0.7	−1.0 ± 1.2	−3.7	−2.0	4.8
K381	−0.5 ± 0.7	−1.7 ± 0.5	−2.2 ± 0.8	−5.0	0.4	2.4
K382ac	−5.3 ± 1.1	−2.6 ± 0.6	−7.9 ± 1.2	−10.8	−11.9	14.8
L383	−3.2 ± 0.7	−2.3 ± 0.6	−5.5 ± 1.0	−4.5	−6.2	5.2
M384	−1.8 ± 0.4	−1.1 ± 0.5	−2.9 ± 0.6	−3.6	−7.4	8.1
F385	−0.7 ± 0.3	0.4 ± 0.6	−0.3 ± 0.7	−2.5	−3.8	5.9
K386	−2.1 ± 1.4	−0.7 ± 0.5	−2.8 ± 1.5	−2.7	−41.7	41.6

Table III

Decomposition of Energetic Contributions (in kcal/mol) from Selected Residues of the CBP Bromodomain

	Side chain	Backbone	Total
L1109	−0.9 ± 0.5	−0.5 ± 0.5	−1.4 ± 0.9
P1110	−0.9 ± 0.3	−0.4 ± 0.1	−1.3 ± 0.3
V1115	−1.3 ± 0.5	−0.2 ± 0.1	−1.5 ± 0.5
L1120	−1.2 ± 0.5	0.0 ± 0.3	−1.2 ± 0.7
G1121	0.0 ± 0.0	−1.1 ± 0.7	−1.1 ± 0.7
I1122	−1.9 ± 0.6	−0.4 ± 0.3	−2.3 ± 0.7
P1123	−0.9 ± 0.4	−0.7 ± 0.2	−1.6 ± 0.5
D1124	−2.3 ± 1.1	−0.2 ± 0.1	−2.5 ± 1.2
Y1167	−1.1 ± 0.4	−1.3 ± 0.5	−2.4 ± 0.6
N1168	−2.4 ± 0.7	−0.5 ± 0.5	−2.9 ± 0.8
S1172	0.2 ± 0.7	−1.8 ± 0.4	−1.6 ± 0.8
R1173	−0.6 ± 0.5	−1.9 ± 0.3	−2.5 ± 0.6
V1174	−2.0 ± 0.7	−0.8 ± 0.3	−2.8 ± 0.8

Energetics of p53-K382ac CBP bromodomain interactions

To gain a better understanding of the origin of the energy of interaction between the K382ac and the binding pocket in CBP bromodomain, we conducted a MM-GBSA decomposition of the interaction energies. In addition to the energetic components of K382ac, we also present the contributions from the other residues of p53 in Table II and those from selected residues of CBP bromodomain in Table III.

Figure 8

Pairwise interactions between p53 and CBP bromodomain. K382ac is observed to interact with almost all residues proximal to the peptide. Notably, we observed interactions with Y1167 (at the backbone) and N1168 (at the side chain). Hydrophobic residues (P1110, V1115, I1122, P1132, M1133, and A1164) have significant contributions through van der Waals interactions, while Q1118 has contribution through backbone electrostatic interactions. Calculating specific pairwise interactions can guide the design of specific small molecules with improved affinity and selectivity.

The results in Table II show that K382ac makes the largest contribution to the interaction energy. The contribution originates from a balance between nearly equal parts from favorable vdW and electrostatic interactions and an unfavorable desolvation of the residue. The total interaction energy of −7.9 kcal/mol comes from a major contribution from the side chain of −5.3 kcal/mol and a smaller portion from the backbone of −2.6 kcal/mol. Interestingly, the contribution from the side chain is very similar to the results obtained from the FEP calculations in which the acetylated lysine was converted to lysine, suggesting that most of the interaction between the side chain and the acetyl-lysine binding pocket originated from the acetyl group. Among the other residues of the p53, Leu-383 makes a large contribution followed by M384 and K381. These contributions are generally in good agreement with the mutational studies of Mujtaba et al.[10] For example, these authors showed that the acetylated p53 at K382 competes against a biotinylated peptide immobilized on streptavidine-agarose beads, whereas the nonacetylated peptide failed to do so. Furthermore, mutating F or M in the p53 AcK382 peptide weakened its binding to the bromodomain, whereas change of H, K, or L caused a nearly complete loss of bromodomain binding. However, it is important to note that since most of the energy of interaction in K381 and L383 comes from the backbone, it appears that the mutated peptides may be binding to CBP bromodomain in a different mode. R379 also makes a large contribution, but the effect of its mutation has not been reported.[10]

Table III summarizes the contributions from selected residues in the CBP bromodomain. The results in the table are consistent with mutational experiments,[10] for example, see Y1167, N1168, and V1115. Most of the residues make larger contributions through their side chains, except Y1167, S1172, and R1173, whose interaction energy comes from the backbone. Although the side chain and backbone of Y1167 contribute nearly equally to the total interaction energy, the major effect of mutating this residue might suggest that in addition to the loss of interaction with the aromatic ring, substantial conformational changes occur in the backbone as well.

Neither the previous analysis nor the mutational experiments provide a specific explanation for the importance of some of the residues whose mutation causes major changes in binding and biological activity. The MM-GBSA analysis can provide a pairwise decomposition of the interaction energy including the changes in solvation of the specific residues upon complex formation. We conducted such an analysis and present the results in Figure 8 for interactions that exceed ∼1 kcal/mol (for specific details see Table II in Supporting Information). The results in Figure 7 clearly show that the K382ac has many interactions with almost all the residues that are proximal to the peptide. The major interactions are with Y1167 and N1168 and while both residues

contribute about the same amount in vdW interactions (−1.2 kcal/mol and −1.5 kcal/mol, respectively), the electrostatic interaction with N1168 is −3.7 kcal/mol mostly from the side chain vs. −1.4 kcal/mol with Y1167 mostly coming from the backbone. Other important interactions are with hydrophobic residues: P1110, V1115, I1122, P1132, M1133, and A1164, and they make major contributions through vdW interactions. Q1118 makes a major contribution through electrostatic interactions, which come mostly from the backbone.

The arrangement of the p53 peptide in the binding groove determines the interaction pattern with the flanking residues around K382ac. H380 interacts with residues in the ZA loop mostly through van der Waals interactions, whereas L383, M384, and F385 interact with the BC loop. These are mostly interactions between the p53 peptide backbone and the side chains of N1168 and R1173. Because the inclusion of entropic effects due to the binding cannot be easily partitioned among the residues of the peptide and the complex, we want to emphasize that such an analysis provides a qualitative description of the relative contributions of various residues to the interaction between the K382ac p53 peptide and the CBP bromodomain. Nevertheless, it is clear that the K382ac plays a major role in this interaction.

CONCLUSIONS

The combination of molecular dynamics simulations with structural and biochemical analysis is a powerful approach to the characterization of specific molecular processes that play an important role in cell-signal modulations. We have demonstrated in this work that the conformational flexibility in the acetylated and nonacetylated p53 peptide does not contribute to the preferential binding of the acetylated form. Adopting the simple approach of conformational selection of the preferred conformation, we showed that the two peptides demonstrate a negligible conformational free energy difference. Because the population of the preferred conformation is of the order of 40–50%, and the sampling of the peptide conformational space in the 40 ns simulations appears to be rather extensive, it is reasonable to assume that inducing a conformational change to increase the bound population will not contribute substantially to the differential energy of binding. These studies clearly focus on the importance of the acetylated lysine as a group with a major contribution to binding.

Our Free Energy Perturbation simulations confirm this conclusion: the contribution of the acetyl group amounts to 4.8 kcal/mol, which is a major portion of the binding energy of the peptide. As noted previously the contributions come from a preferred set of favorable van der Waals interactions. The unfavorable electrostatics

originates both from a set of repulsions and a larger cost of desolvation of the nonacetylated group.

The decomposition of the interaction energies into residue-based contributions shows very good agreement with mutational experiments. Interestingly, the contributions from the side chain of the K382ac are similar to those obtained in FEP calculations. Furthermore, this analysis points to the relative role of the flanking residues in the peptide as well as of those in the CBP bromodomain. These conclusions are in line with the observations from mutational experiments and they corroborate the conclusions drawn from the structural studies. The pairwise decomposition, however, offers additional information, which may be difficult to obtain from simple mutational experiments. Such an analysis explicitly pairs the interactions between residues in the peptide with those in the CBP bromodomain presenting an opportunity to observe the affinity modulation of other peptides with a different sequence and interpret the observed changes. Lastly, the understanding of the physical forces behind the specific pairwise interactions can guide the design of specific small molecules with improved affinity and selectivity. The ability of such small molecules to potentially alter the binding and biological activity of bromodomains may ultimately bring us closer to the concept of designing efficient synthetic chemical switches for use in dedicated therapeutic intervention.

REFERENCES

1. Strachan T, Read AP. Human molecular genetics. New York; Oxford: Wiley-Liss: BIOS Scientific Publishers; 1999. p 576.
2. Levine AJ. p53, the cellular gatekeeper for growth and division. Cell 1997;88:323–331.
3. Kern SE, Kinzler KW, Bruskin A, Jarosz D, Friedman P, Prives C, Vogelstein B. Identification of p53 as a sequence-specific DNA-binding protein. Science 1991;252:1708–1711.
4. Jackson-Grusby L, Beard C, Possemato R, Tudor M, Fambrough D, Csankovszki G, Dausman J, Lee P, Wilson C, Lander E, Jaenisch R. Loss of genomic methylation causes p53-dependent apoptosis and epigenetic deregulation. Nat Genet 2001;27:31–39.
5. Arkin MR, Wells JA. Small-molecule inhibitors of protein-protein interactions: progressing towards the dream. Nat Rev Drug Discov 2004;3:301–317.
6. Lohrum MA, Vousden KH. Regulation and activation of p53 and its family members. Cell Death Differ 1999;6:1162–1168.
7. Rodriguez MS, Desterro JM, Lain S, Lane DP, Hay RT. Multiple C-terminal lysine residues target p53 for ubiquitin-proteasome-mediated degradation. Mol Cell Biol 2000;20:8458–8467.
8. Geyer RK, Yu ZK, Maki CG. The MDM2 RING-finger domain is required to promote p53 nuclear export. Nat Cell Biol 2000;2:569–573.
9. Woods DB, Vousden KH. Regulation of p53 function. Exp Cell Res 2001;264:56–66.
10. Mujtaba S, Zeng L, Zhou MM. Structure and acetyl-lysine recognition of the bromodomain. Oncogene 2007;26:5521–5527.
11. Zeng L, Zhang Q, Gerona-Navarro G, Moshkina N, Zhou MM. Structural basis of site-specific histone recognition by the bromodomains of human coactivators PCAF and CBP/p300. Structure 2008; 16:643–652.
12. Manning ET, Ikehara T, Ito T, Kadonaga JT, Kraus WL. p300 forms a stable, template-committed complex with chromatin: role for the bromodomain. Mol Cell Biol 2001;21:3876–3887.
13. Travers A. Chromatin modification: how to put a HAT on the histones. Curr Biol 1999;9:23–25.
14. Barlev NA, Liu L, Chehab NH, Mansfield K, Harris KG, Halazonetis TD, Berger SL. Acetylation of p53 activates transcription through recruitment of coactivators/histone acetyltransferases. Mol Cell 2001; 8:1243–1254.
15. Mujtaba S, He Y, Zeng L, Yan S, Plotnikova O, Sachchidanand , Sanchez R, Zeleznik-Le NJ, Ronai Z, Zhou MM. Structural mechanism of the bromodomain of the coactivator CBP in p53 transcriptional activation. Mol Cell 2004;13:251–263.
16. Sachchidanand, Resnick-Silverman L, Yan S, Mutjaba S, Liu WJ, Zeng L, Manfredi JJ, Zhou MM. Target structure-based discovery of small molecules that block human p53 and CREB binding protein association. Chem Biol 2006;13:81–90.
17. Liu H, Duan Y. Effects of posttranslational modifications on the structure and dynamics of histone H3 N-terminal peptide. Biophys J 2008;94:4579–4585.
18. Kollman PA, Massova I, Reyes C, Kuhn B, Huo S, Chong L, Lee M, Lee T, Duan Y, Wang W, Donini O, Cieplak P, Srinivasan J, Case DA, Cheatham TE, III. Calculating structures and free energies of complex molecules: combining molecular mechanics and continuum models. Acc Chem Res 2000;33:889–897.
19. Cheatham TE, III, Srinivasan J, Case DA, Kollman PA. Molecular dynamics and continuum solvent studies of the stability of polyG-polyC and polyA-polyT DNA duplexes in solution. J Biomol Struct Dyn 1998;16:265–280.
20. Phillips JC, Braun R, Wang W, Gumbart J, Tajkhorshid E, Villa E, Chipot C, Skeel RD, Kale L, Schulten K. Scalable molecular dynamics with NAMD. J Comput Chem 2005;26:1781–1802.
21. MacKerell AD, Jr, Banavali N, Foloppe N. Development and current status of the CHARMM force field for nucleic acids. Biopolymers 2000;56:257–265.
22. Humphrey W, Dalke A, Schulten K. VMD: visual molecular dynamics. J Mol Graph 1996;14:33–38.
23. Ryckaert JP, Ciccotti G, Berendsen HJC. Numerical integration of the cartesian equations of motion of a system with constraints: molecular dynamics of n-alkanes. J Comput Phys 1977;23:327–341.
24. Mezei M. Simulaid, simulation setup utilities. URL:http://atlas.physbio.mssm.edu/~mezei/simulaid/simulaid.html. 2006; 2007.
25. Ramachandran GN, Sasiskharan V. Conformation of polypeptides and proteins. Adv Protein Chem 1968;23:283–437.
26. Kabsch W. A solution of the best rotation to relate two sets of vectors. Acta Crystallogr 1976;32:922–923.
27. Hénin J, Chipot C. A tutorial for alchemical FEP in NAMD. URL: http://www.ks.uiuc.edu/Research/namd/tutorial/fep/. Volume2008: Theoretical and Computational Biophysics Group; 2008.
28. Rodriguez Y, Mezei M, Osman R. The PT1-Ca(2+) Gla domain binds to a membrane through two Dipalmitoylphosphatidylserines. A computational study (dagger). Biochemistry 2008;47:13267–13278.
29. Gohlke H, Case DA. Converging free energy estimates: MM-PB(GB)SA studies on the protein-protein complex Ras-Raf. J Comput Chem 2004;25:238–250.
30. Gohlke H, Kiel C, Case DA. Insights into protein-protein binding by binding free energy calculation and free energy decomposition for the Ras-Raf and Ras-RalGDS complexes. J Mol Biol 2003;330: 891–913.
31. Ravishanker G, Swaminathan S, Beveridge DL, Lavery R, Sklenar H. Conformational and helicoidal analysis of 30 PS of molecular dynamics on the d(CGCGAATTCGCG) double helix: "curves," dials and windows. J Biomol Struct Dyn 1989;6:669–699.
32. Chandrasekaran R, Thompson M. Polybromo-1-bromodomains bind histone H3 at specific acetyl-lysine positions. Biochem Biophys Res Commun 2007;355:661–666.